Identification of nuclear pore proteins at plasmodesmata

T. Moritz Schladt[1,2,*], Manuel Miras[1,2,8,*], Jona Obinna Ejike[1,2,*], Mathieu Pottier[1,2,9,*], Lin Xi[3], Andrea Restrepo-Escobar[1,2], Masayoshi Nakamura[4], Niklas Pütz[1,2], Sebastian Hänsch[2,5], Chen Gao[1,2], Julia Engelhorn[1,2], Marcel Dickmanns[1,2,6], Gwendolyn V. Davis[1,2], Ahan Dalal[1,2], Sven Gombos[3], Ronja Lange[1,2], Rüdiger Simon[2,7], Waltraud X. Schulze[3] & Wolf B. Frommer[1,2,4,§]

[1] Heinrich Heine University Düsseldorf, Faculty of Mathematics and Natural Sciences, Institute for Molecular Physiology, Düsseldorf, Germany
[2] Cluster of Excellence on Plant Sciences, Heinrich Heine University Düsseldorf, Germany
[3] Department of Plant Systems Biology, University of Hohenheim, 70593 Stuttgart, Germany
[4] Institute for Transformative Biomolecules (WPI-ITbM), Nagoya University, Nagoya, Japan
[5] Center for Advanced Imaging; Heinrich Heine University Düsseldorf, Düsseldorf, Germany
[6] Department of Molecular Structural Biology, Max Planck Institute of Biochemistry, Martinsried, Germany
[7] Heinrich Heine University Düsseldorf, Faculty of Mathematics and Natural Sciences, Institute of Developmental Genetics, Germany
[8] New address: Department of Stress Biology and Plant Pathology, CEBAS-CSIC, Murcia, Spain
[9] New address: Université de Lorraine, INRAE, IAM, F-54000 Nancy, France

* Equal contribution
§ For correspondence: frommew@hhu.de

Summary

Plasmodesmata (PD) exchange small molecules, RNAs and proteins between plant cells with an exclusion limit for passive, non-specific transport. PD also facilitate the transport of specific cargo that may require chaperones or carriers for transport. The mechanisms underlying PD transport are not understood. PD and nuclear pore complexes (NPC), are nanometer size micropores with similar transport properties. The permeability barrier in NPCs is a phase separation domain formed by FG-nucleoporins (FG-NUP). Here we used bioinformatics, proteomics and fluorescence imaging to identify proteins with similarities to phase separating FG-NUPs at PD. We identified 20 NUPs in PD fractions, and validated dual localization to NPC and PD for 7 NUPs. Structured illumination microscopy detected the transmembrane anchor NUP CPR5 at both orifices of PD. *cpr5* mutants showed reduced intercellular transport of SHR from stele to endodermis. The identification of FG-NUPs at PD is consistent with the recruitment of NUPs in the green lineage to form a PD pore gating complex consistent with liquid phase separation domains as diffusion barriers at PD.

Introduction

Nutrient exchange and communication between cells are essential for multicellular organisms. Besides transporters and cell surface receptors, metazoa, fungi and plants independently evolved cell-cell bridges. The green lineage developed unique structures, called plasmodesmata (PD), composed of modified cell wall domains that form plasma membrane-lined channels and contain an ER-derived desmotubule to generate continuity between the cytoplasm of neighboring cells. Since PD are embedded into the cell wall and likely contain diverse membrane and soluble proteins, PD pose a major challenge for biochemical and cell biological analyses. Several studies obtained PD proteomes by enriching membrane proteins in cell wall fractions[1–4]. Genetic approaches have so far failed to identify genes that could fully explain the transport mechanism, possibly due to redundancy or lethality. Transport studies are also challenging since intact multicellular systems are required for analyses.

Key features of PD transport appear to be the ability to translocate highly diverse cargo (from ions to macromolecules), a size exclusion limit (which, depending of the type of PD, can reach 70 kDa, in funnel PD up to 120 kDa), and the ability to translocate specific cargo[5,6]. Lee et al. highlighted that transport through PD and the nuclear pore complex (NPC) share common features[7], namely both NPC and PD transport a similar spectrum of cargo species (ions, metabolites, proteins, and ribonucleoprotein complexes). For both NPC and PD, the ability for pore dilation has been described[8,9]. Both NPC and PD constitute selective barriers, allowing '*passive passage of molecules'* with an apparent size exclusion limit (term used in animal literature; named '*non-targeted movement*' for PD) and '*facilitated translocation of specific macromolecules'* ('*targeted movement*' for PD)[10,11]. Surface properties of cargo proteins appear to play an important role, thus at least for nuclei, there is no strict size exclusion limit[11]. The core of the permeability barrier of the NPC appears to be a separated phase or condensate formed by disordered phenylalanine–glycine (FG) repeat-containing proteins, which function as 'smart sieves' and produce phase-separated domains in a good Flory solvent-like environment *in situ*[11–14]. These smart sieves mediate passage of smaller molecules and proteins without interaction with the FG repeats, while larger molecules or specific cargo can pass with the help of nuclear transport receptors (NTR) that interact with the FG repeats[15]. As a shared structure among eukaryotes, the ultrastructure, function and transport mechanism of the NPC is well understood[16]. The human NPC, with about 1000 polypeptides, has a diameter of 120 nm, a pore size of ~43 nm and a height of 80 nm and is composed of a membrane-anchor, three stacked rings (a sandwich of two outer and an inner ring), cytoplasmic filaments, and a nucleocytoplasmic basket[17].

FG-NUPs and other NUPs in PD fractions of *Physcomitrium patens* and Arabidopsis

Based on similar features, we hypothesized that the PD transport mechanism could involve FG-repeat proteins that generate a liquid phase separation domain in PD with properties similar as the NPC. We thus explored whether the green lineage evolved a distinct set of FG-repeat containing proteins. The human genome encodes twelve FG-nucleoporins (NUPs): NUP42, NUP50, NUP54, NUP58 (aka NUP45), NUP62, NUP98, NUP153, NUP214, POM121, POM121B, POM121C, and NUP358[18], while plant genomes encode ten FG-NUPs: NUP42 (aka CG1), NUP50a & NUP50b, NUP54, NUP58, NUP62, NUP98a & NUP98b, NUP136 and NUP214[19,20]. The majority of the FG-NUPs were conserved, with only three FG-NUPs lost in the green lineage (NUP153, POM121, NUP358). A bioinformatic search for FG repeat-containing proteins in the genome of the moss *P. patens* revealed that 12 out of the 15 top-ranked FG-containing proteins were NUPs; the other three proteins were not considered candidates for a transport function (table S1; file S1; file S2 for Arabidopsis FG-containing proteins). An alternative hypothesis was that the PD permeability barrier is generated by NUPs derived by tandem gene duplications followed by differentiation into NPC and PD functions. However, phylogenetic analyses showed that the majority of NUPs are encoded by single genes (table S2)[20,21]. Notably, an analysis of the PD proteome from *P. patens* identified FG-NUP50a and two other NUPs, SEC13 and NUA[1]. Our previous work had indicated that moss PD proteins can be targeted to PD when expressed in tobacco leaves, indicating conservation of the targeting signals[1]. To test whether FG-NUPs localize exclusively to the NPC or can also be targeted to PD, the subcellular localization of fluorescent protein (FP) fusions of three *P. patens* FG-NUPs (NUP58, NUP62 and NUP98) was analyzed by confocal microscopy after estradiol-controlled transient expression in *Nicotiana benthamiana*. A substantial number of fluorescent puncta derived from C-terminal mVenus fusions of the three FG-NUPs overlaid with fluorescent puncta of aniline blue marking callose at PD (Fig.

1A; fig. S1). PD localization did not appear to be due to an FG-NUPs-specific mis-localization, since the inner ring linker NUP35, which connects the transmembrane interaction hub with the ALADIN-NDC1 core to NUP155, also localized to PD (Fig. 1A).

To obtain independent evidence, and to explore whether FG-NUPs may also be present in PD fractions from a vascular plant, we utilized established PD enrichment and data analysis pipelines to generate a PD proteome from Arabidopsis shoots[1]. This shoot PD proteome had an overlap of 80% with published PD proteomes and included ~43% of known high-confidence PD proteins, e.g., the well-established PDLP and MCTP PD markers (table S3, fig. S2, S3, file S3)[2,22]. Notably, seven Arabidopsis FG-NUPs were identified in the PD fraction (Fig. 1B). In addition, inner and outer ring and basket NUPs were found in the high-confidence PD protein list (Fig. 1B). In total, 20 proteins covering different domains of the NPC were identified, and 15 were enriched in PD fractions compared to cell wall and total Arabidopsis protein fractions (Fig. 1B, C, fig. S2, S3). Several of the identified nuclear pore components passed the threshold for consideration as high-confidence PD proteins, in particular proteins of the inner and outer rings, core and basket. Three FG-NUPs NUP62, NUP214, NUP50a, as well as CPR5, GP210, NUP35, NUP93a, NUP155, NUP205, NUP43, HOS1 (aka HOS1/ELYS), SEC13, and NUP82 were also found in proteomics data of cell wall/PD protein fractions from other studies (table S4)[1,3,4,23,24].

Localization of Arabidopsis FG-NUPs and other NUPs to PD

To explore whether Arabidopsis FG-NUP-mVenus fusions can be detected at PD by confocal microscopy, candidates were expressed from an estradiol-inducible promoter in *N. benthamiana* leaves, which can be used to limit overexpression. Fluorescence derived from FP-fusions of the FG-NUP58, FG-NUP62 and FG-NUP98b overlaid with aniline blue fluorescent puncta (with a significantly higher PD index relative to that for the non-specific cell wall dye propidium iodide, Fig. 2, fig S4, table S2), indicating that Arabidopsis FG-NUPs can also be targeted to PD in this system. Notably, 12 out of a total of the 16 NUPs tested here localized to puncta in the cell periphery that overlaid with aniline blue fluorescence at pit fields (Fig. 2, Fig. 3A, B; fig. S4)[25]. Overall, 12 NUPs showed significant enrichment at PD compared to the cell wall marker (Fig. 2B, Fig. 3B, table S2). Among them were two outer ring NUPs (NUP43, HOS1/ELYS) and two transmembrane NUPs (GP210, CPR5) (Fig. 1C, 3B). As expected, ten NUP fusions for various inner and outer ring and membrane anchor NUPs were also detected in nuclei (fig. S4, list of 16 tested NUPs: table S2). Fluorescent puncta of aniline blue and FP-fusions of PD protein typically do not provide a perfect colocalization since aniline blue staining does not mark all PD and typically, the overlay is partial since FP-fusions are not detected at all PD even for high confidence PD proteins[26]. As an independent measure, overlay of the PD marker PDLP5-mScarlet3 and an mCitrine fusion of the putative NUP107-160 complex recruitment factor HOS1/ELYS at PD was validated (Fig. 3C). To test for potential artifacts, caused possibly by mistargeting due to overexpression, both the concentration of the inducer estradiol and the induction time were reduced, leading to a drop in overall fluorescence intensity, however, without negatively affecting dual NUP localization (here NUP43-mCitrine) at NPC and PD (Fig. 3D). Single copy insertions of GFP-fusions are likely to avoid overexpression. Analysis of nine independent stably transformed homozygous single insertion Arabidopsis lines expressing a full-length genomic FG-NUP62-GFP fusion showed dual localization to nuclei and PD in cotyledons (Fig. 2 C, D). Arabidopsis FG-NUP62 had previously shown to form hydrogels that recapitulate the NPCs phase separation-like transport properties *in vitro*[27]. The results are in line with the hypothesis of FG-repeat based phase separation domains as a permeability barrier at PD[27]. Other components of the NPC located at PD could provide a scaffold that holds the FG-NUPs in place in a yet to be determined structure. Notably, in contrast to C-terminal FP fusions of the auto-cleavable NUP98a[28], here, a C-terminal NUP98b-mVenus fusion produced fluorescence at PD (Fig. 2, fig. S4), indicating that either the main fraction of NUP98b in the study by Gallemi et al. (2016) was unprocessed, or that the C-terminal peptide reassociated with the N-terminal domain of NUP98b, as previously described for the two splice forms of the human NUP98[29]. Out of 16 NUPs tested, four NUPs did not localize at PD, as indicated by p-values >0.08 (table S2). Out of 35 currently known Arabidopsis NUPs, 19 NUPs were not yet tested here (table S2). In summary, our data indicate that NUPs of the non-vascular moss *P. patens* and the vascular plant Arabidopsis can dually localize to NPC and PD, including the plant-specific membrane anchor CPR5 and FG-NUP NUP62. Components

of the inner ring, NUP93a and NUP155, and the basket, NUP82, were also detected at PD, although with lower confidence compared to, e.g., CPR5. Analysis of published data from other groups who had localized NUPs to nuclei also showed peripheral puncta, which had not been analyzed further (table S5). While it is conceivable that NUPs may contain distinct NPC and PD targeting sequences, alternatively they might be recruited to the two locations as preformed subcomplexes by a common receptor or anchor to assemble a pore that harbors a phase separation domain and constitutes a permeability barrier.

Topology of CPR5, a potential membrane anchor at both NPC and PD

Since the phase separation domain in the nuclear pore is produced by ten FG-NUPs and PD appear to contain multiple FG-NUPs, it may be necessary to mutate multiple *FG-NUP* genes before it is possible to observe intercellular transport defects. It is also conceivable that, *knock-out* mutants in multiple *FG-NUPs* may be lethal. We therefore focused on the green lineage-specific membrane anchor CPR5, a nuclear pore component with a PD index of 1.48 (Fig. 3, table S2). Four potential membrane proteins that anchor the human NPC in the nuclear membrane had been identified: GP210, POM121, NDC1 and TMEM33. Arabidopsis encodes genes for three anchors GP210, NDC1 and PNET1 (homologue of human TMEM209) (table S6), while CPR5 had been proposed to serve as an anchor in the equatorial plane of the NPC[30]. Since CPR5 was among the top 5 candidates based on the PD index, one may hypothesize that it contributes to anchoring an NPC-like structure at PD (Fig. 3A, B, fig. S4). CPR5, a polytopic membrane protein, is predicted to form a globular helix bundle domain at its N-terminus, flanked by disordered regions and connected to a 105 amino acid α-helix (fig. S5). The central helix contains a hydrophobic region, which, together with four shorter hydrophobic helices, forms an approximately 35 Å long transmembrane domain, consistent with the expected thickness of ER membranes. The C-terminus possibly extends into the ER lumen. CPR5 may play a specialized role in the plant NPC or serve as a replacement for the missing metazoan POM121[31]. CPR5 is encoded as a single gene in Arabidopsis and two in rice (fig. S6, table S6, table S7)[32].

Principal differences between the NPC and PD are the overall length (nuclear double membrane thickness at the pore ～30 nm; PD, length depends on cell wall thickness, between 100 nm and several μm), the presence of a nuclear double-membrane *vs*. two separate membranes at PD, i.e., an outer plasma membrane and an ER-like desmotubule in the center of the pore. In PD, CPR5 could either be embedded into the PD plasma membrane, with the C-terminus facing the apoplasm, or into the ER/desmotubule membrane, with its C-terminus facing the desmotubule lumen and the long N-terminal domain pointing into the intermembrane space of PD, analogous to the CPR5 topology in the ER-derived nuclear membrane at the NPC. A split-GFP system for topology studies of membrane proteins was used to determine whether the C-terminus of CPR5 faces the luminal side of the ER[33]. When an N-terminal GFP11 fusion to CPR5 was co-expressed with a free cytosolic GFP1-10, fluorescence was reconstituted, consistent with the N-terminus located in the cytosol sleeve of PD (Fig. 4A; fig. S7). A control using a GFP1-10 domain targeted to and retained in the ER lumen (GFP1-10-HDEL) did not show detectable fluorescence reconstitution (Fig. 4B). The complementary fusion of GFP11 to the C-terminus of CPR5 led to reconstitution of fluorescence when co-expressed with an ER lumen targeted GFP1-10-HDEL, but not when co-expressed with a cytosolic GFP1-10 (Fig. 4A, B; fig. S7). The topological data are consistent with a model in which the C-terminal five-helix-bundle of CPR5 traverses the ER/desmotubule membrane with the C-terminus inside the lumen of the ER/desmotubule, while the extended central α-helix, the predicted unstructured domains, and the smaller helical bundle of CPR5 are located in the intermembrane space between the ER/desmotubule and the plasma membrane (fig. S5).

Localization of CPR5 at the orifices of PD

A hypothetical NPC-like structure could serve as a micropore in the PD channel, or be present on PD entrance. To determine CPR5 localization in the PD at higher resolution, we performed structured illumination microscopy (SIM) with a CPR5-mCitrine fusion. CPR5 localized to the neck region of PD adjacent to aniline blue labeled callose deposition (Fig. 4C, D; fig. S8), but not in the central cavity of the PD, where PDLP5-mScarlet3 was localized[34]. These findings are consistent with a model in which NUPs are present at the PD orifices. We did not observe puncta at both paired neck regions in all cases (fig.

S8B, top), possibly due to mosaic-like expression in *N. benthamiana*, in which only one of the adjacent cells expressed the fusion protein (model: Fig. 4D).

Intercellular transport defects in *cpr5* mutants

If indeed NUPs form condensates at PD to control cell-to-cell transport, and given the defects of *cpr5* mutants in nuclear transport, one may expect that interference with CPR5 function might impair *facilitated and non-facilitated cell-to-cell translocation of specific macromolecules*. Particle bombardment of Arabidopsis leaves was performed to transiently express a tandem-GFP fusion (2xmEGFP; 54 kDa) in two independent *cpr5* loss-of-function mutants (EMS mutant *cpr5-1* (G420D) and T-DNA insertion mutant *cpr5-T3*[35,36];fig. S9C, D)[30,35–40] uncovered defects in cell-to-cell transport. Cell-to-cell movement of 2xmEGFP was significantly reduced in the *cpr5* mutants relative to WT (Fig. 5A, B; fig. S9A, B). Originally named for its *constitutive pathogen response* phenotype, loss of CPR5 activity can trigger constitutive defense responses that could cause callose deposition and closure of PD [41], however, callose levels were not significantly different (Fig. 5C). The transcription factor SHORT-ROOT (SHR), produced in cells of the stele, migrates into the endodermis by *facilitated cell-to-cell translocation,* followed by nuclear import[42]. Intercellular transport of SHR is crucial for tissue patterning[42–44]. To explore whether SHR-GFP (86.6 kDa) movement was impacted in a *cpr5* loss-of-function mutant, we compared the endodermis-to-stele ratio (E:S ratio) of GFP fluorescence intensity in roots of homozygous *shr* mutants expressing pSHR:SHR–GFP in wild type (WT) as well as in the *cpr5-1* mutant background. The E:S ratio was significantly reduced in *cpr5-1* compared to WT, consistent with a defect in facilitated SHR transport across PD (Fig. 5D, E). Fluorescence recovery after photobleaching (FRAP) of nuclei in the root endodermis of homozygous *shr*/pSHR:SHR lines in *cpr5-1* was significantly lower compared to WT, further supporting that targeted transport across PD is reduced in *cpr5-1* (Fig. 5F,G, fig. S9F). Notably, no significant difference in SHR–GFP fluorescence intensity was observed in the steles of WT versus *cpr5-1* lines (fig. S9E). The *cpr5* mutants showed no detectable defect in small molecule transport indicates WT-like PD density and retention of the capability to mediate small molecule transport as shown by Drop-ANd-See *trans*-leaf diffusion assays (DANS, carboxyfluorescein: 376 Da; control CaMV*35S:PDLP5*; Fig. 5H, I)[45]. Localization of CPR5 to PD, and the specific defects in macromolecular non-targeted and targeted transport may implicate a role of CPR5 in PD transport.

Potential roles for NUPs at PD

Based on the observations (i) that NUPs were identified in PD-enriched cell wall fractions, (ii) that 12/35 known plant NUPs, and in particular FG-NUPs, localized to PD, and (iii) that intercellular tandem-GFP and SHR transport was reduced in *cpr5* mutants may indicate that components of the NPC may generate a complex that can sustain a similar liquid phase separation domain at PD as found in the NPC, and that liquid phase separation generated by FG-NUPs may play a role in intercellular translocation[15]. The exact composition and structure of the predicted plasmodesmatal pore complex (PDPC), and how dual targeting is achieved, remains to be explored. The insights gained here may open new ways to understand the structure, function, transport mechanism and regulation of PD and how to engineer the permeability barrier between cells.

References

1. Gombos, S. *et al.* A high-confidence *Physcomitrium patens* plasmodesmata proteome by iterative scoring and validation reveals diversification of cell wall proteins during evolution. *New Phytol.* **238**, 637–653 (2023).
2. Brault, M. L. *et al.* Multiple C2 domains and transmembrane region proteins (MCTPs) tether membranes at plasmodesmata. *EMBO Rep.* **20**, e47182 (2019).
3. Fernandez-Calvino, L. *et al.* Arabidopsis plasmodesmal proteome. *PloS One* **6**, e18880 (2011).
4. Bayer, E. M. *et al.* Arabidopsis cell wall proteome defined using multidimensional protein identification technology. *PROTEOMICS* **6**, 301–311 (2006).

5. Paultre, D. S. G., Gustin, M.-P., Molnar, A. & Oparka, K. J. Lost in transit: long-distance trafficking and phloem unloading of protein signals in Arabidopsis homografts. *Plant Cell* **28**, 2016–2025 (2016).

6. Ross-Elliott, T. J. *et al.* Phloem unloading in Arabidopsis roots is convective and regulated by the phloem-pole pericycle. *eLife* **6**, e24125 (2017).

7. Lee, J. Y., Yoo, B. C. & Lucas, W. J. Parallels between nuclear-pore and plasmodesmal trafficking of information molecules. *Planta* **210**, 177–187 (2000).

8. Zimmerli, C. E. *et al.* Nuclear pores dilate and constrict in cellulo. *Science* **374**, eabd9776 (2021).

9. Kragler, F., Monzer, J., Shash, K., Xoconostle-Cázares, B. & Lucas, W. J. Cell-to-cell transport of proteins: requirement for unfolding and characterization of binding to a putative plasmodesmal receptor. *Plant J.* **15**, 367–381 (1998).

10. Crawford, K. M. & Zambryski, P. C. Non-targeted and targeted protein movement through plasmodesmata in leaves in different developmental and physiological states. *Plant Physiol.* **125**, 1802–1812 (2001).

11. Frey, S. *et al.* Surface properties determining passage rates of proteins through nuclear pores. *Cell* **174**, 202-217.e9 (2018).

12. Ng, S. C., Güttler, T. & Görlich, D. Recapitulation of selective nuclear import and export with a perfectly repeated 12mer GLFG peptide. *Nat. Commun.* **12**, 4047 (2021).

13. Hoogenboom, B. W. *et al.* Physics of the nuclear pore complex: Theory, modeling and experiment. *Phys. Rep.* **921**, 1–53 (2021).

14. Yu, M. *et al.* Visualizing the disordered nuclear transport machinery in situ. *Nature* **617**, 162–169 (2023).

15. Kehlenbach, R. H., Neumann, P., Ficner, R. & Dickmanns, A. Interaction of nucleoporins with nuclear transport receptors: a structural perspective. *Biol. Chem.* **404**, 791–805 (2023).

16. Mosalaganti, S. *et al.* AI-based structure prediction empowers integrative structural analysis of human nuclear pores. *Science* **376**, eabm9506 (2022).

17. Lin, D. H. & Hoelz, A. The structure of the nuclear pore complex (an update). *Annu. Rev. Biochem.* **88**, 725–783 (2019).

18. Terry, L. J. & Wente, S. R. Flexible gates: dynamic topologies and functions for FG nucleoporins in nucleocytoplasmic transport. *Eukaryot. Cell* **8**, 1814–1827 (2009).

19. Chopra, K., Bawaria, S. & Chauhan, R. Evolutionary divergence of the nuclear pore complex from fungi to metazoans. *Protein Sci.* **28**, 571–586 (2019).

20. Makarov, A. A., Padilla-Mejia, N. E. & Field, M. C. Evolution and diversification of the nuclear pore complex. *Biochem. Soc. Trans.* **49**, 1601–1619 (2021).

21. Zhang, C. *et al.* Genomic identification and expression analysis of nuclear pore proteins in *Malus domestica*. *Sci. Rep.* **10**, 17426 (2020).

22. Thomas, C. L., Bayer, E. M., Ritzenthaler, C., Fernandez-Calvino, L. & Maule, A. J. Specific targeting of a plasmodesmal protein affecting cell-to-cell communication. *PLoS Biol.* **6**, e7 (2008).

23. Kraner, M. E., Müller, C. & Sonnewald, U. Comparative proteomic profiling of the choline transporter-like1 (CHER1) mutant provides insights into plasmodesmata composition of fully developed *Arabidopsis thaliana* leaves. *Plant J. Cell Mol. Biol.* **92**, 696–709 (2017).

24. Kirk, P., Amsbury, S., German, L., Gaudioso-Pedraza, R. & Benitez-Alfonso, Y. A comparative meta-proteomic pipeline for the identification of plasmodesmata proteins and regulatory conditions in diverse plant species. *BMC Biol.* **20**, 128 (2022).

25. Zavaliev, R. & Epel, B. L. Imaging callose at plasmodesmata using aniline blue: quantitative confocal microscopy. *Methods Mol. Biol. Clifton NJ* **1217**, 105–119 (2015).

26. Pendle, A. & Benitez-Alfonso, Y. Immunofluorescence detection of callose deposition around plasmodesmata sites. *Methods Mol. Biol. Clifton NJ* **1217**, 95–104 (2015).

27. Wang, J. *et al.* Phase separation of the nuclear pore complex facilitates selective nuclear transport to regulate plant defense against pathogen and pest invasion. *Mol. Plant* **16**, 1016–1030 (2023).

28. Gallemí, M. *et al.* DRACULA2 is a dynamic nucleoporin with a role in regulating the shade avoidance syndrome in Arabidopsis. *Development* **143**, 1623–1631 (2016).

29. Hodel, A. E. *et al.* The three-dimensional structure of the autoproteolytic, nuclear pore-targeting domain of the human nucleoporin Nup98. *Mol. Cell* **10**, 347–358 (2002).

30. Gu, Y. *et al.* Nuclear pore permeabilization is a convergent signaling event in effector-triggered immunity. *Cell* **166**, 1526-1538.e11 (2016).

31. Apelt, L. *et al.* Systematic protein–protein interaction analysis reveals intersubcomplex contacts in the Nuclear Pore Complex. *Mol. Cell. Proteomics MCP* **15**, 2594–2606 (2016).

32. Arra, Y. *et al.* Rice Yellow Mottle Virus resistance by genome editing of the *Oryza sativa L. ssp. japonica* nucleoporin gene *OsCPR5.1* but not *OsCPR5.2*. *Plant Biotechnol. J.* **22**, 1299–1311 (2024).

33. Xie, W., Nielsen, M. E., Pedersen, C. & Thordal-Christensen, H. A split-GFP gateway cloning system for topology analyses of membrane proteins in plants. *PLOS ONE* **12**, e0170118 (2017).

34. Fitzgibbon, J., Bell, K., King, E. & Oparka, K. Super-resolution imaging of plasmodesmata using three-dimensional structured illumination microscopy. *Plant Physiol.* **153**, 1453–63 (2010).

35. Wang, F. *et al.* Arabidopsis CPR5 regulates ethylene signaling via molecular association with the ETR1 receptor. *J. Integr. Plant Biol.* **59**, 810–824 (2017).

36. Bowling, S. A., Clarke, J. D., Liu, Y., Klessig, D. F. & Dong, X. The cpr5 mutant of Arabidopsis expresses both NPR1-dependent and NPR1-independent resistance. *Plant Cell* **9**, 1573–84 (1997).

37. Crawford, K. M. & Zambryski, P. C. Subcellular localization determines the availability of non-targeted proteins to plasmodesmatal transport. *Curr. Biol.* **10**, 1032–1040 (2000).

38. Faulkner, C. *et al.* LYM2-dependent chitin perception limits molecular flux via plasmodesmata. *Proc. Natl. Acad. Sci.* **110**, 9166–9170 (2013).

39. Sakulkoo, W. *et al.* A single fungal MAP kinase controls plant cell-to-cell invasion by the rice blast fungus. *Science* **359**, 1399–1403 (2018).

40. Otero, S., Helariutta, Y. & Benitez-Alfonso, Y. Symplastic communication in organ formation and tissue patterning. *Curr. Opin. Plant Biol.* **29**, 21–28 (2016).

41. Kohler, A., Schwindling, S. & Conrath, U. Benzothiadiazole-induced priming for potentiated responses to pathogen infection, wounding, and infiltration of water into leaves requires the *NPR1/NIM1* gene in Arabidopsis. *Plant Physiol.* **128**, 1046–1056 (2002).

42. Nakajima, K., Sena, G., Nawy, T. & Benfey, P. N. Intercellular movement of the putative transcription factor SHR in root patterning. *Nature* **413**, 307–311 (2001).

43. Koizumi, K., Hayashi, T., Wu, S. & Gallagher, K. L. The SHORT-ROOT protein acts as a mobile, dose-dependent signal in patterning the ground tissue. *Proc. Natl. Acad. Sci. U. S. A.* **109**, 13010–13015 (2012).

44. Winter, C. M. *et al.* SHR and SCR coordinate root patterning and growth early in the cell cycle. *Nature* 1–6 (2024) doi:10.1038/s41586-023-06971-z.

45. Lee, J.-Y. *et al.* A plasmodesmata-localized protein mediates crosstalk between cell-to-cell communication and innate immunity in Arabidopsis. *Plant Cell* **23**, 3353–3373 (2011).

Acknowledgments

We would like to dedicate this manuscript to the 'champion of plasmodesmata', William J. (Bill) Lucas (UC Davis). We thank Madlen Somsich (HHU) for project coordination and management and Anita Snyder (www.anitaksnyder.com) for copyediting. This work has received funding from the European Research Council (ERC) and the Marie Skłodowska-Curie Actions under the European Union's Horizon 2020 research and innovation programme (Grant agreements 'SymPore' No. 951292 to WBF and "PDgate" No. 101023981 to MM, respectively). This research was also supported by the Deutsche Forschungsgemeinschaft (DFG, German Research Foundation) under Germany´s Excellence Strategy – EXC-2048/1 – project ID 390686111, and the Alexander von Humboldt Professorship, to WBF.

Data availability

Source data will be deposited at Dryad. Sequencing data for strains from this study have been deposited in the NCBI Sequence Read Archive (SRA) database under the accession codes will be provided at the time of publication. Materials will be made available under MTA; some materials were obtained from others as marked and require permission from the respective authors.

Contributions

WBF conceived of the study. J.E. performed the bioinformatic analyses; L.X., S.G. and W.S. performed proteomics and data analysis; M.D. analyzed the structure and generated fig. S4; S.H. helped to establish and advised on SIM. T.M.S, M.P., M.M., J.O.E., N.P., M.N., G.V.D, C.G. and A.D. performed imaging and/or transport studies; R.S. advised on imaging and data analyses; M.M. and A.R-E. performed split GFP studies, T.M.S, M.M., M.P., J.O.E., B.S., and W.B.F. analyzed the data; T.M.S., M.M., M.P., J.O.E., G.V.D, R.S. and W.B.F. wrote the manuscript.

Competing interests

We declare no competing interests.

Supplementary Materials

- Material and Methods
- 8 Supplementary Tables
- 10 Supplementary Figures
- 3 Supplementary files
- 2 Supplemental scripts
- Supplementary references

Figures and legends

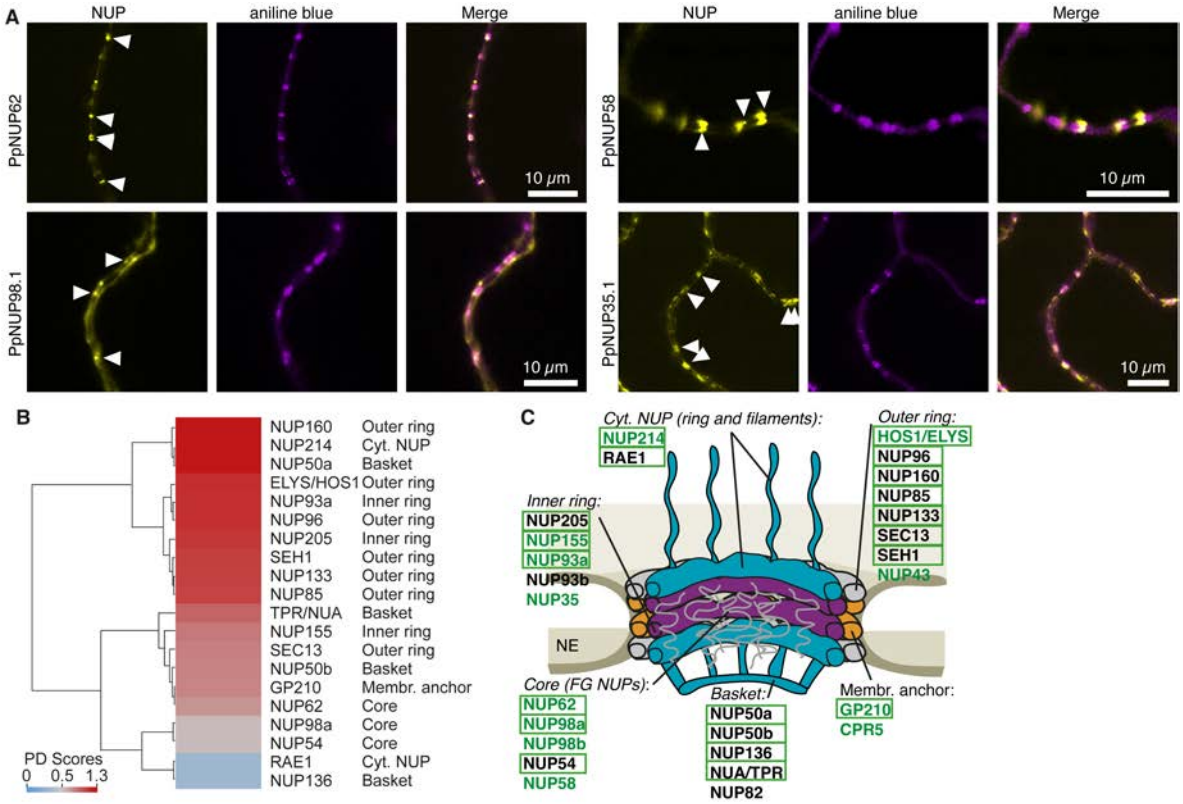

Figure 1. Identification of NUPs at plasmodesmata. (**A)** Localization of NUPs from *Physcomitrium patens* at PD. **(B)** Hierarchical clustering of PD scores of Arabidopsis NPC components found in PD proteome preparations from 5-week-old Arabidopsis shoot tissues. Clustering based on Euclidean distance of PD scores, which were averages of at least three replicate scores from separate tissue preparations. Color scale represents PD score values. PD scores above the high-confidence threshold of 0.5 are indicated in shades of red. (**C)** Scheme of an NPC embedded in the nuclear envelope with all NUPs studied in this work. NUPs listed in B are green boxed. NUPs found to be significantly enriched at PD in the transient localization assay (Fig. 2B, 3B) are written in green letters. Corresponding AGI locus identifiers in table S2. Cytoplasmic NUP is abbreviated as Cyt. NUP, and membrane anchor as Membr. anchor.

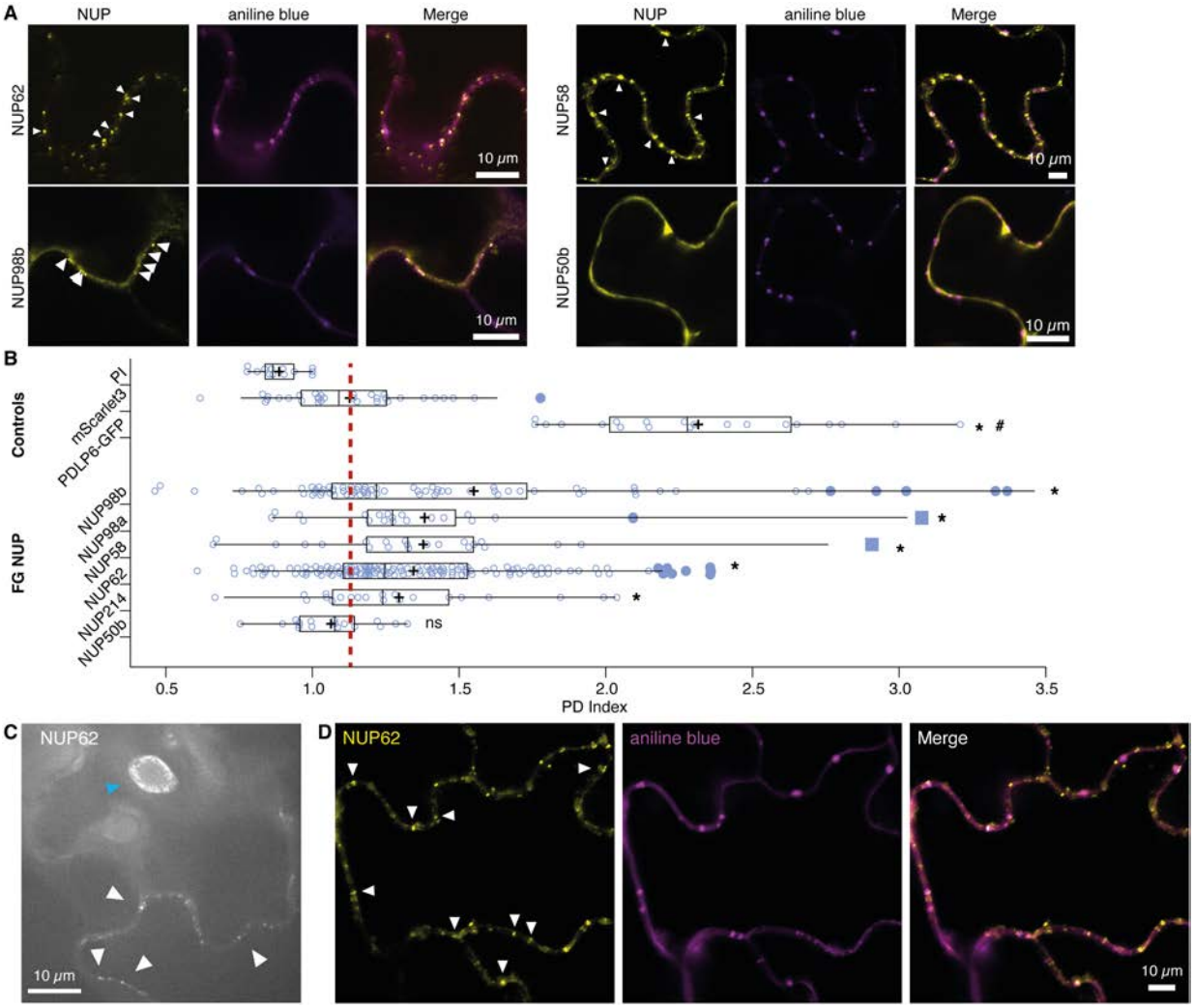

Figure 2. Analysis of the localization of Arabidopsis FG NUPs to PD. (A) Localization of selected Arabidopsis FG-NUPs after transient expression under the control of the estradiol-inducible XVE promotor in *N. benthamiana* epidermal cells using confocal microscopy. mVenus was fused to the C-terminus of different NUPs, except for Nup98a for which GFP was fused both N- and C-terminally (GFP-NUP98a-GFP). Aniline blue was infiltrated to detect callose in pit fields as an indicator of plasmodesmata. Localization was repeated in three independent experiments with similar results. (**B**) Quantification of the PD localization by PD index. Red dashed line indicates the mean PD index of mScarlet3 (cytoplasmic control). PI, propidium iodide ('membrane impermeant dye'). Significantly ($p < 0.05$) increased PD indices compared to the cell wall or cytoplasmic controls are indicated by * and #, respectively. Kruskal-Wallis Test $p = < 0.001$, p-values of Bonferroni corrected pairwise test are summarized in table S2. Median is represented by vertical line inside the box, mean is represented by the bold +. Values between quartiles 1 and 3 are represented by box ranges, and 5th and 95th percentile are represented by error bars. At least 15 images from 3 biological replicates were analyzed for each NUP. Independent localization data are shown in fig. S3. (**C and D**) Arabidopsis NUP62-GFP plant expressing NUP62 fused to GFP under its own promoter. (**C**) The localization of NUP62-GFP in 12-day-old cotyledon epidermal cells was visualized by confocal microscopy using a confocal unit CSU10 with a 100x oil-immersion lens. Blue arrowhead for nuclear localization, white arrowheads for peripheral localization of NUP-62-GFP. **(D)** Localization of NUP62-GFP in a 12-day-old cotyledon epidermal cell of stably transformed Arabidopsis line. The cotyledon was immersed in aniline blue to detect callose in pit fields as an indicator of plasmodesmata. White arrowheads in D indicate overlay of NUPs and aniline blue. Scale bar: 10 µm.

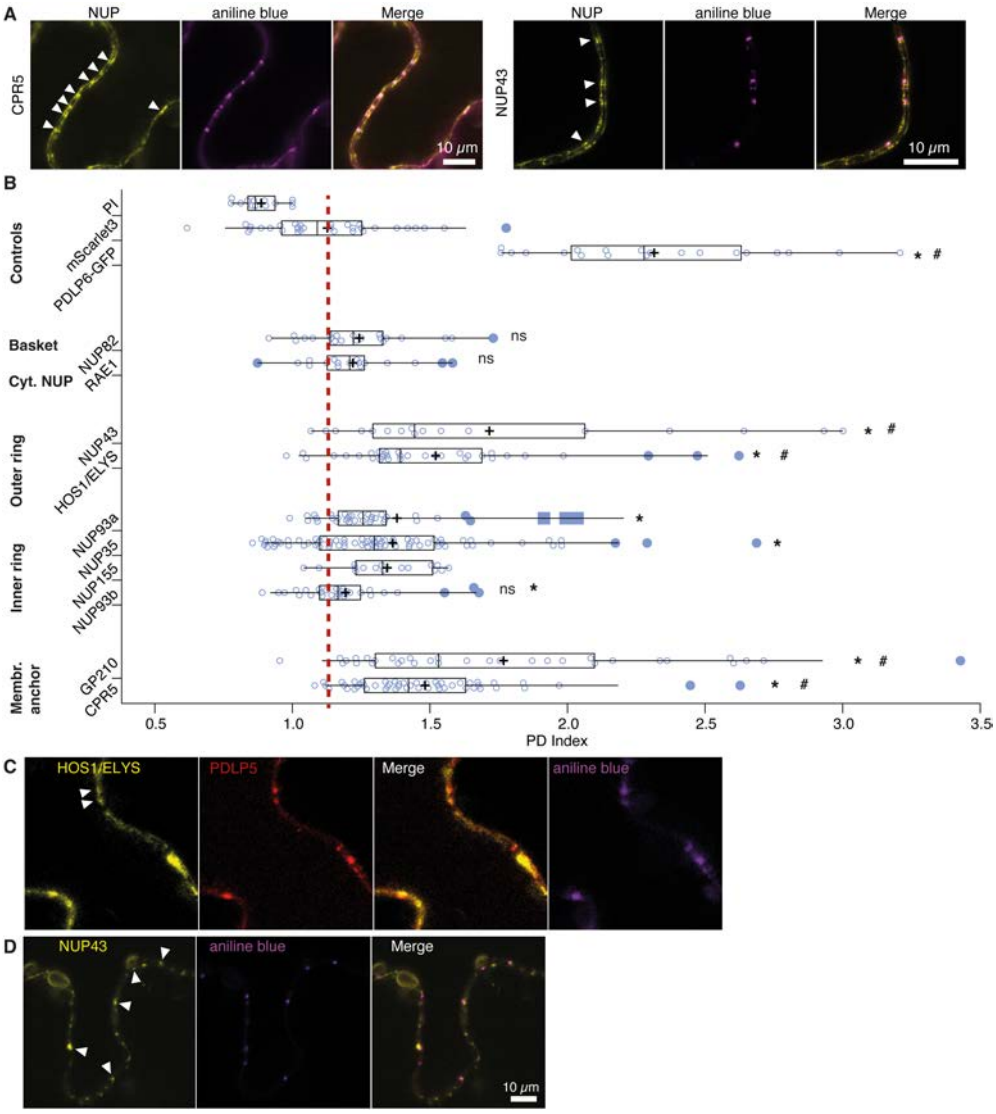

Figure 3. Dual localization of Arabidopsis scaffold and transmembrane NUPs. (A) Localization of Arabidopsis transmembrane (CPR5) and scaffold (NUP43) NUPs after transient expression under the control of the estradiol-inducible XVE promotor in *N. benthamiana* epidermal cells using confocal microscopy. mVenus was fused to the C-terminus of different NUPs. Aniline blue was infiltrated to detect callose in pit fields as an indicator of plasmodesmata. White arrowheads indicate overlay with aniline blue. Localization was repeated in three independent experiments with similar results. (**B**) Quantification of the PD localization by PD index. Red dashed line indicates the mean PD index of mScarlet3 (cytoplasmic control). PI, propidium iodide ('membrane impermeant dye'). Significantly ($p < 0.05$) increased PD indices compared to the cell wall or cytoplasmic controls are indicated by * and #, respectively. Kruskal-Wallis Test $p < 0.001$, p-values of Bonferroni corrected pairwise test are summarized in table S2. Median is represented by vertical line inside the box, mean is represented by the bold +. Values between quartiles 1 and 3 are represented by box ranges, and 5th and 95th percentile are represented by error bars. At least 15 images from 3 biological replicates were analyzed for each NUP. Independent localization data are shown in fig. S3. Control identical to Fig. 2B. (**C**) Localization of HOS1/ELYS-mCitrine and PDLP5-mScarlet3 expressed transiently under the control of the inducible XVE promotor in *N. benthamiana* epidermal cells. Aniline blue was infiltrated to stain callose that accumulates in pit fields. White arrowheads indicate overlay of HOS1/ELYS-mCitrine and PDLP5-mScarlet3 channel. The localization pattern has been repeated in three independent experiments with similar results. **(D)** NUP43-mCitrine localization at PD at 1/10 estradiol concentration and shortened induction time. White arrowheads indicate overlay with aniline blue.

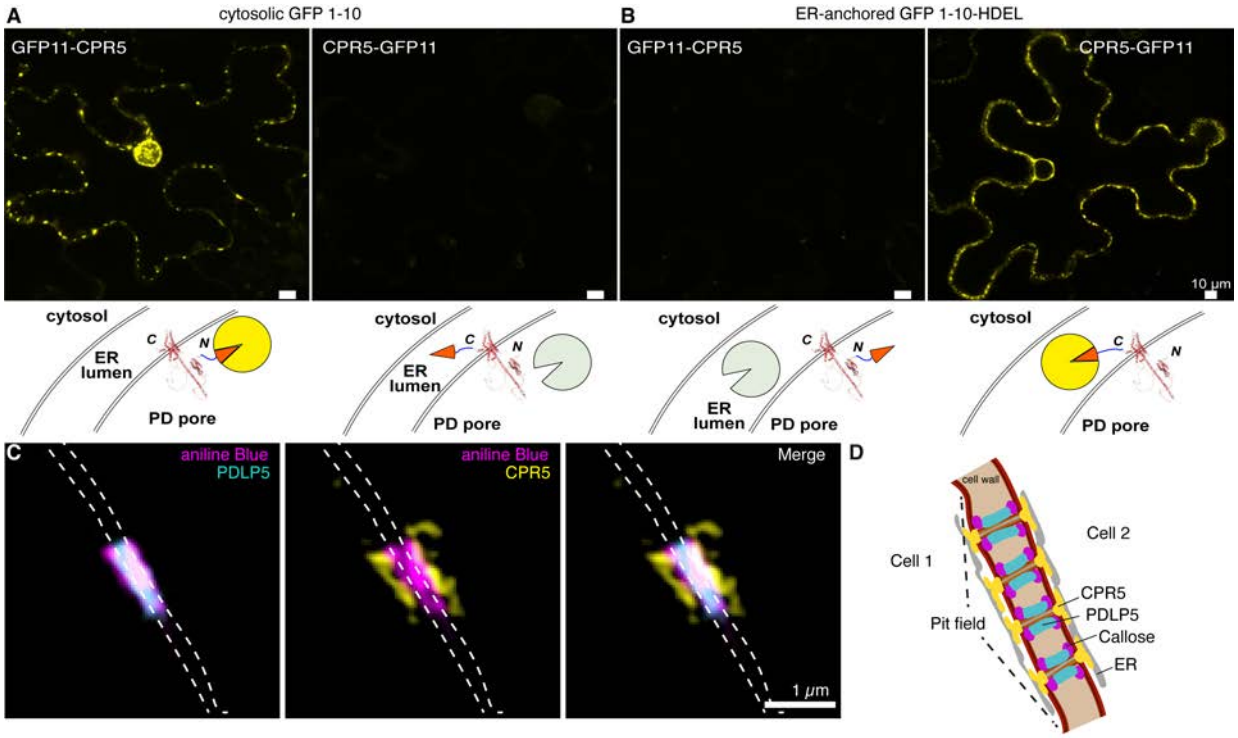

Figure 4. CPR5 topology and localization of CPR5 near PD orifices. Split-GFP membrane topology to test for the orientation of CPR5 in the nuclear pore membrane and the ER at PD. (**A**) *(left)* Fluorescence reconstitution at PD between a cytosolic non-fluorescent GFP domain lacking β-sheet 11 (GFP1-10; the circle missing a wedge) and a fusion of the GFP11 to the N-terminus of CPR5 (the red wedge). Since reconstitution occurs at PD, each cartoon indicates reconstitution in the intermembrane space between ER/desmotubule and plasma membrane. *(right)* Absence of fluorescence reconstitution between a cytosolic GFP1-10 and the fusion of the GFP11 to the C-terminus of CPR5. (**B**) *(left)* Absence of fluorescence reconstitution between an ER-retained GFP1-10-HDEL and a fusion of GFP11 to the N-terminus of CPR5. *(right)* Fluorescence reconstitution at PD between an ER-retained GFP1-10-HDEL and a fusion of the GFP11 to the C-terminus of CPR5. Repeated independently 3 times with comparable results. (**C**) Detection of CPR5-mCitrine close to the orifices of PD by Structured Illumination Microscopy (SIM) of *N. benthamiana* leaves co-infiltrated with XVE:PDLP5-mScarlet3 and XVE:CPR5-mCitrine. Prior to the imaging, leaves were infiltrated with aniline blue. PDLP5-mScarlet3 in turquoise, CPR5-mCitrine in yellow, and aniline blue in magenta. Repeated independently four times with comparable results. **(D)** Cartoon approximately to scale, illustrating plasmodesmata in a pitfield between two adjacent cells with callose marked in purple, PDLP5 in magenta and CPR5 in yellow.

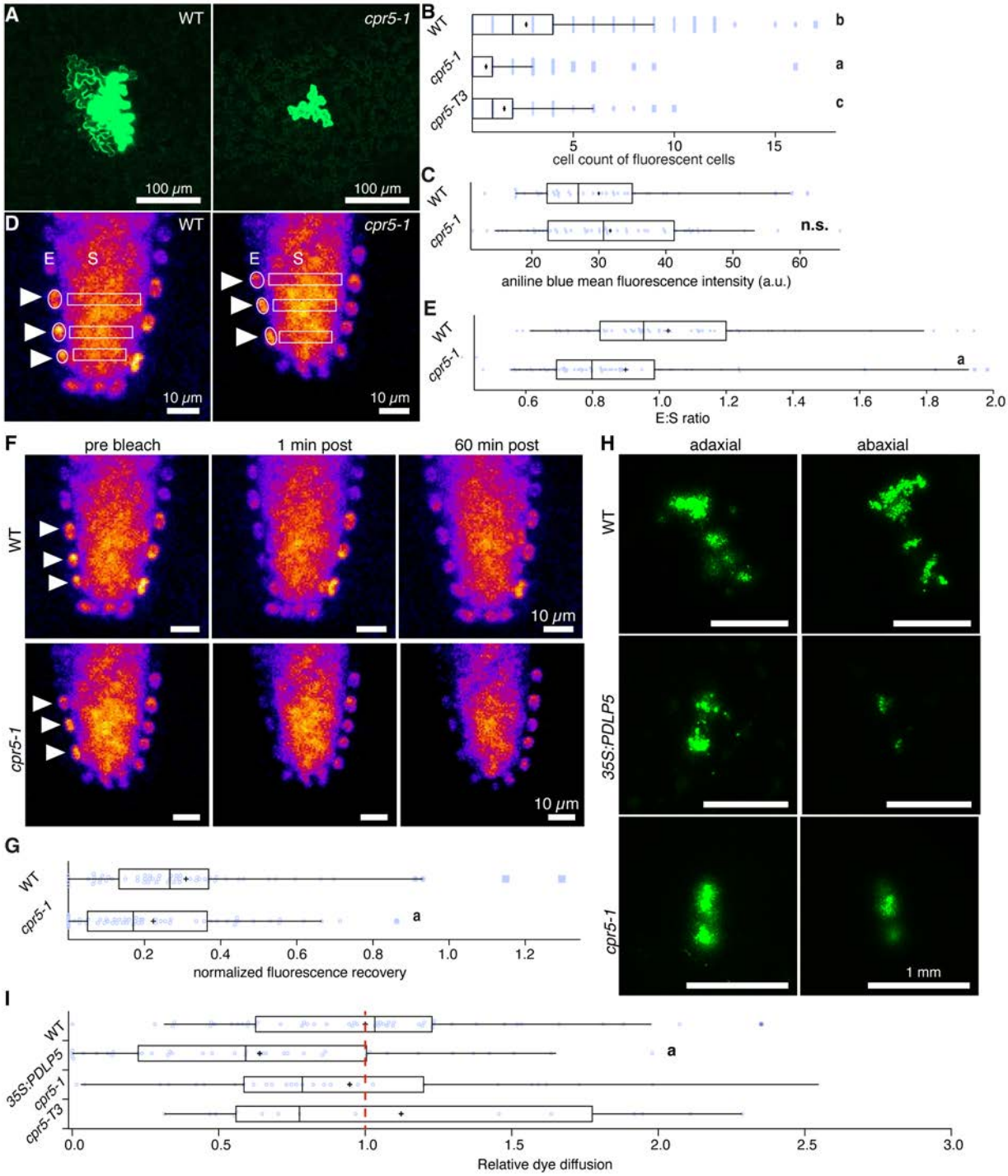

Figure 5. Defects in cell-to-cell transport of kDa-sized cargo in *cpr5* mutants. (A) Example images of intercellular 2xmEGFP movement in wild type (WT, *left*) and *cpr5-1* (*right*) Arabidopsis leaves. Leaves were bombarded with gold particles coated with p35S:mEGFP-mEGFP DNA plasmids 24 h prior to the experiment (fusion protein abbreviated as 2xmEGFP). **(B)** Quantification of the intercellular spread of mEGFP by counting fluorescent cells in the GFP channel. $n_{(WT)}$ = 594 bombarded cells, 17 independent biological replicates. $n_{(cpr5\text{-}1)}$ = 278 bombarded cells, 6 independent biological replicates. $n_{(cpr5\text{-}T3)}$ = 99 bombarded cells, four independent biological replicates. **a** indicates significant difference to WT with $p_{(cpr5\text{-}T3)} = 0.0004$; **b** indicates significant difference to WT with $p_{(cpr5\text{-}1)} < 10^{-15}$; $p_{(cpr5\text{-}1 \text{ vs. } cpr5\text{-}T3)} = 0.0002$ (Kruskal-Wallis test with Bonferroni correction for pairwise comparison). **(C)** Callose quantification. $n_{(WT)}$ = 4 independent experiments, $n_{(cpr5\text{-}1)}$ = 5 independent experiments, graph summarizes all experiments. Student´s *t*-test $p = 0.48$. **(D)** Sum projections showing SHR–GFP distribution in WT (*left*) and *cpr5-1* mutant (*right*) root. White circles and boxes indicate positions of endodermis nuclei (E,

arrows) and corresponding regions in the stele (S, white boxes). **(E)** Quantification of SHR–GFP endodermis:stele ratio (E:S) for WT and *cpr5-1* mutant. $n_{(WT)}$ = 62 nuclei, $n_{(cpr5\text{-}1)}$ = 62 nuclei, with 3-4 nuclei analyzed per root. **a** indicates significantly decreased E:S in *cpr5-1* mutant, based on Mann-Whitney U test with $p = 0.0006$. **(F)**, Sum projections showing SHR–GFP distribution in WT (*top*) and *cpr5-1* (*bottom*) background. **(G)**, Quantification of relative SHR–GFP fluorescence recovery for WT and *cpr5-1* mutant after 1 h. Fluorescence recovery was normalized to a control nucleus in the endodermis (see Methods and fig. S9F). n(WT) = 59 bleached nuclei, n(*cpr5-1*) = 59, per root 3-4 nuclei were bleached. Student´s t-test p = 0.037 indicating significantly decreased fluorescence recovery after 60 min. **(H and I)** PD permeabilities examined by CFDA/CFSE-based DANS dye loading assays. **(H)** Epifluorescence reporting on CF diffusion in the epidermis of the adaxial (*left*) and abaxial (*right*) side of the leaf. WT *(top), 35S*:*PDLP5* (*middle*), and *cpr5-1* (*bottom*). Bars, 1 mm. **(I)** Quantification of CF diffusion in WT and mutant lines. $n_{(WT)}$ = 49 plants, 7 independent biological replicates; $n_{(35S:PDLP5)}$ = 38 plants, 5 independent biological replicates; $n_{(cpr5\text{-}1)}$ = 29 plants, 5 independent biological replicates; $n_{(cpr5\text{-}T3)}$ = 15 plants, 5 independent biological replicates. Fluorescent areas on the abaxial side were identified using auto threshold and Fiji YEN-algorithm with user modifications. The same threshold setting was used for the adaxial side. The extent of dye diffusion was quantified by the ratio between the areal spread of fluorescence on the abaxial side and the areal spread of fluorescence on the adaxial side. **a** indicates significantly different at the $\alpha = 0.032$ level according to Bonferroni-corrected pair wise comparison following Kruskal-Wallis analysis.